Antiviral Research 151 (2018) 78–86

Contents lists available at ScienceDirect

Antiviral Research

journal homepage: www.elsevier.com/locate/antiviral

# Discovery of a non-nucleoside RNA polymerase inhibitor for blocking Zika virus replication through *in silico* screening

Aryamav Pattnaik[a], Nicholas Palermo[b], Bikash R. Sahoo[a], Zhe Yuan[c], Duoyi Hu[a], Arun S. Annamalai[a], Hiep L.X. Vu[d,f], Ignacio Correas[a], Pavan Kumar Prathipati[e], Christopher J. Destache[e,f], Qingsheng Li[c,f], Fernando A. Osorio[a,f], Asit K. Pattnaik[a,f,*,1], Shi-hua Xiang[a,f,*,1]

[a] School of Veterinary Medicine and Biomedical Sciences, University of Nebraska-Lincoln, USA
[b] Holland Computing Center, University of Nebraska-Lincolns, USA
[c] School of Biological Sciences, University of Nebraska-Lincoln, USA
[d] Department of Animal Sciences, University of Nebraska-Lincoln, USA
[e] School of Pharmacy and Health Professions, Creighton University, Omaha, NE 68178, USA
[f] Nebraska Center for Virology, University of Nebraska-Lincoln, Lincoln, NE 68583, USA

ARTICLE INFO

*Keywords:*
*In silico* screening
Zika virus (ZIKV)
RNA-dependent-RNA polymerase (RdRp)
Non-nucleoside inhibitor (NNI)
TPB

ABSTRACT

Zika virus (ZIKV), an emerging arbovirus, has become a major human health concern globally due to its association with congenital abnormalities and neurological diseases. Licensed vaccines or antivirals against ZIKV are currently unavailable. Here, by employing a structure-based approach targeting the ZIKV RNA-dependent RNA polymerase (RdRp), we conducted *in silico* screening of a library of 100,000 small molecules and tested the top ten lead compounds for their ability to inhibit the virus replication in cell-based *in vitro* assays. One compound, 3-chloro-N-[({4-[4-(2-thienylcarbonyl)-1-piperazinyl]phenyl}amino)carbonothioyl]-1-benzothiophene-2-carboxamide (TPB), potently inhibited ZIKV replication at sub-micromolar concentrations. Molecular docking analysis suggests that TPB binds to the catalytic active site of the RdRp and therefore likely blocks the viral RNA synthesis by an allosteric effect. The $IC_{50}$ and the $CC_{50}$ of TPB in Vero cells were 94 nM and 19.4 μM, respectively, yielding a high selective index of 206. In *in vivo* studies using immunocompetent mice, TPB reduced ZIKV viremia significantly, indicating TPB as a potential drug candidate for ZIKV infections.

## 1. Introduction

Zika virus (ZIKV), a mosquito-borne pathogen, was originally isolated in Uganda in 1947 (Dick et al., 1952) and only sporadic cases of virus outbreaks in humans were reported in Africa and Asia in the next six decades (Mecharles et al., 2016; Munoz et al., 2016). However, in the past ten years, it has rapidly emerged and spread to the regions of Asia, Europe, and the Americas (Aliota et al., 2017; Chan et al., 2016; Deseda, 2017; Weaver et al., 2016). Although the majority of infections in humans are asymptomatic, recent ZIKV infections have been linked to a variety of congenital disorders including microcephaly and fetal growth restriction (Carteaux et al., 2016; Cauchemez et al., 2016; Chan et al., 2016; Coyne and Lazear, 2016; Cugola et al., 2016; Lazear and Diamond, 2016; Miner and Diamond, 2017; Mlakar et al., 2016) as well as Guillain-Barre syndrome in adults (Avelino-Silva and Martin, 2016; Nascimento et al., 2017; Parra et al., 2016). These severe consequences and the large-scale spreading of the virus have imposed a significant threat to human health worldwide (Fauci and Morens, 2016; Gulland, 2016; Roos, 2016). So far, no vaccine or drug for preventing or treating this viral disease is available (Shan et al., 2016). Therefore, it is urgent to develop countermeasures against this viral epidemic (Rather et al., 2017; Salam et al., 2017).

ZIKV is classified into the genus Flavivirus in the family *Flaviviridae*, which is similar to Dengue virus (DENV), West Nile virus (WNV), Japanese encephalitis virus (JEV) and Yellow fever virus (YFV). It has a single positive-strand RNA genome of ~11 kilobases and replicates using viral RNA-dependent RNA polymerase (RdRp). Since the RdRp is a key enzyme for ZIKV replication, it is an attractive target for antiviral

* Corresponding authors. Nebraska Center for Virology, School of Veterinary Medicine and Biomedical Sciences, University of Nebraska-Lincoln, Morrison Center 337, 4240 Fair Street, Lincoln, NE 68583-09, USA.
*E-mail addresses:* apattnaik2@unl.edu (A.K. Pattnaik), sxiang2@unl.edu (S.-h. Xiang).
[1] These authors contributed equally to the work.

https://doi.org/10.1016/j.antiviral.2017.12.016
Received 12 October 2017; Received in revised form 12 December 2017; Accepted 20 December 2017
Available online 21 December 2017
0166-3542/ © 2017 Elsevier B.V. All rights reserved.

drug development (Duan et al., 2017; Ramharack and Soliman, 2017; Wang et al., 2017). During replication, the viral positive-sense RNA genome is translated into a single polypeptide that is subsequently cleaved by viral and host proteinases to generate three structural proteins (capsid, C; precursor membrane, PrM; and envelope, E) and seven non-structural (NS) proteins (NS1, NS2A, NS2B, NS3, NS4A, NS4B, and NS5) (Baronti et al., 2014; Perera and Kuhn, 2008). The NS5 is the most conserved among the NS proteins and contains two domains: the methyltransferase (MTase) domain at the N-terminus (residues 1–264) and the RdRp domain at the C-terminus (residues 275–903). The MTase is required for mRNA capping and stabilization to facilitate translation process, to escape detection of the viral mRNA by the host innate immune sensors as well as for cap-independent methylation with yet unknown functions (Coutard et al., 2017), whereas the RdRp domain is required for RNA synthesis. The structure of ZIKV RdRp, like other RdRps of flaviviruses, adopts a typical right-hand shape architecture which includes three subdomains: fingers, thumb and palm (Duan et al., 2017; Godoy et al., 2017; Upadhyay et al., 2017; Zhao et al., 2017). A large cavity is formed at the junction of the three subdomains. The cavity contains the catalytic site for RNA polymerization, RNA entry and exit channels, and NTP entry channel as well as a large priming loop which plays an important role in regulating RNA synthesis and elongation. This large cavity in the RdRp of other viruses has become a major target for antiviral drug development (Choi and Rossmann, 2009; Duan et al., 2017; Shi and Gao, 2017). We have chosen this cavity in ZIKV RdRp for structure-based drug design. *In silico* screening approach was employed to search for compounds that target this large cavity. Here, we identify a small molecule compound that inhibits ZIKV replication with high potency and propose its potential as a drug candidate for further development against ZIKV.

## 2. Materials and methods

### 2.1. Compounds

Ten lead compounds (Table 1) were purchased from Hit2Lead Company (ChemBridge Corporation, San Diego, California). Each compound was dissolved in dimethyl sulfoxide (DMSO) to prepare stock solutions of 10 mM and 1 mM and was stored at −20 °C. The compound 1 (c1) used in this research is 3-chloro-N-[({4-[4-(2-**t**hienylcarbonyl)-1-**p**iperazinyl]phenyl}amino)carbonothioyl]-1-**b**enzothiophene-2-carboxamide (TPB). Based on $^{1}$H NMR and LC-MS (ELSD, DAD 200–400 nm, MSD APCI positive) analyses by the provider, the compound is ≥ 95% pure. Mycophenolic acid (MPA) and Ivermectin (IVM) were purchased from Sigma (St. Louis, MO) and resuspended in DMSO to prepare stock solutions. All the compounds used have ≥95% purity.

### 2.2. Cells and viruses

Vero (*Cercopithecus aethiops*, CCL-81), HTR-8/SVneo human trophoblast (CRL-3271), and NTERA-2 human embryonal carcinoma (CRL-1973) cells were obtained from ATCC. The cells were grown and maintained in Dulbecco's modified Eagle's medium (DMEM) containing 10% heat-inactivated fetal bovine serum (FBS) and penicillin/streptomycin (PS) in humidified chamber with 5% $CO_2$ at 37 °C. Zika virus strain PRVABC59 and MR766 were obtained from Barbara Johnson and Brandy Russell at the Centers for Disease Control and Prevention, Fort Collins, Colorado, USA. The viruses were passaged once in Vero cells to prepare stocks and were stored at −80 °C in small aliquots. Titers of the stock viruses were determined by plaque assay using Vero cells as described previously (Annamalai et al., 2017).

**Table 1**
Docking scores of the top 10 compounds.

| Compound | Molecular Weight | Score |
|---|---|---|
| 1 | 541.108 | −118.794 |
| 2 | 455.528 | −118.36 |
| 3 | 525.572 | −118.358 |
| 4 | 516.638 | −118.097 |
| 5 | 476.480 | −117.319 |
| 6 | 539.618 | −116.087 |
| 7 | 484.618 | −115.823 |
| 8 | 471.592 | −115.789 |
| 9 | 471.574 | −115.724 |
| 10 | 482.443 | −114.333 |

### 2.3. Molecular modeling and in silico screening

The ZIKV RdRp structure was modeled based on sequence homology using Modeller 9 program (Webb and Sali, 2014). The DENV-3 RdRp structure (PDB: 2J7U) (Yap et al., 2007) was used as the template. *In silico* screening was performed using Molegro Virtual Docker (MVD) (Molegro ApS, Aarhus, Denmark). The docking site was defined using a ray-tracing algorithm. This resulted in a cavity with a volume of approximately 1034 cubic Å. A receptor grid was built within this cavity with a resolution of 0.2 Å and a radius of 13 Å from the geometric center of the cavity in the ZIKV RdRp model. A 100,000 compound library from ChemBridge (Chembridge DIVERSet™ Chemical Library, ChemBridge Corporation, San Diego, California) was used for this virtual screening. All structural analysis were conducted in the Discovery Studio 4.0 (Biovia, San Diego, CA).

### 2.4. Inhibition assays

Vero cells were seeded in a 96-well plate with the density of 6000 cells per well. In the initial screening study, the compound (1 μM)-virus (0.1 PFU/cell) mixture in virus growth medium (VGM) [DMEM containing 2%FBS, PS, 20 mM hydroxyethyl piperazine ethane sulfonic acid (HEPES), 1 mM sodium pyruvate, and non-essential amino acids] was added to the cells and incubated for 72 h. In a separate experiment conducted using 12-well plates, the cells were first infected with the virus at 0.1 PFU/cell and following adsorption, the cells were washed twice in PBS and incubated in VGM containing 1 μM concentrations of the drugs. The cell culture media were collected at 72–96 h post-infection and assayed for infectious virus by plaque assay and viral genome copies by quantitative RT-PCR. In all subsequent studies, cells in 12-well plates were infected with ZIKV at MOI of 0.1 PFU/cell and following virus adsorption for 1 h at 37 °C, VGM containing various concentrations TPB was added to the cells and incubated as above. Clarified supernatants from the infected cells were then used to determine infectious virus or genome copies as above.

### 2.5. ATP-based cell viability assay

A modified ATP based cytopathic effect (CPE) assay was used for this study based on the CPE method for anti-DENV drug development described previously (Che et al., 2009). Vero cells (approximately 30,000 per well) were seeded in a black 96-well plate for 24 h before the experiment. Cell monolayers were treated with various concentrations of the drugs for 4 days at 37 °C. The ATP concentration was measured following manufacturer's recommendations using CellTiter-Glo kit from Promega (Madison, Wisconsin). Luminescence was recorded using a Veritas Microplate Luminometer at 420 nm. The 50% cytotoxic concentration ($CC_{50}$) was calculated by a non-linear regression analysis of the dose-response curves.

### 2.6. Quantitative real time RT-PCR

ZIKV viral RNA was detected using RT-qPCR on a C100 Thermal Cycler and the CFX96 Real-Time system (Bio-Rad). Viral RNA (vRNA) was extracted from culture supernatant using a QIAamp Viral RNA Mini

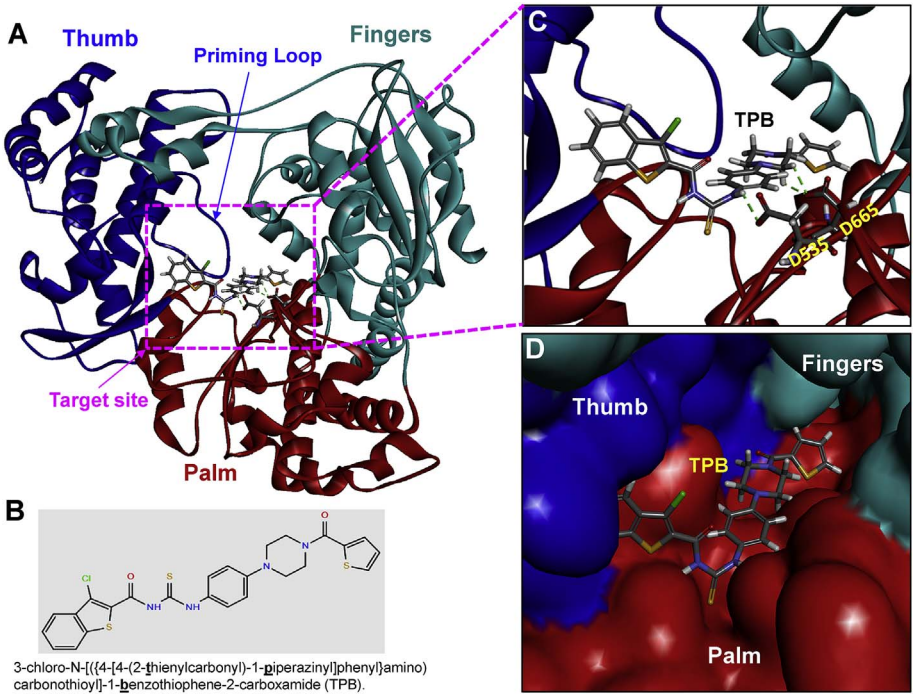


**Fig. 1.** Structure-based screening of inhibitors of ZIKV targeting the viral RNA-dependent RNA-polymerase (RdRp). (A) Structure of ZIKV RdRp generated by homology modeling. The three subdomains are colored individually, Fingers (cyan), Thumb (blue) and Palm (red). The catalytic active site and the priming loop are labeled. Docking of TPB on the active site of RdRp and the contacts with the two aspartic residues (D535 and D665) along with the three hydrogen bonds are indicated. (B) The chemical structure of TPB (molecular weight of 541.108). (C) A larger view of the boxed area in A is shown for clarity. (D) The space-filing model of the boxed area in A is shown along with the bound TPB. TPB binding at the palm subdomain is shown.

kit (Qiagen) and TaqMan Fast Virus 1-Step Master Mix (Life technologies) (Yuan et al., 2016). ZIKV primers and probe (ZIK-F:CCGCTGCCCAACACAAG; ZIK-R:CCACTAACGTTCTTTTGCAGACAT; PCR Probe: ZIK-P: AGCCTACCTTGACAAGCAATCAGACACTCAA) were used for quantitative RT-PCR (RT-qPCR) with the following parameters: 50 °C 30min, 95 °C 5min, (95 °C 30 S, 58 °C 1min) X 40 cycles. RNA standard concentrations were determined based on the back calculation with OD values and molecular weights and were generated through serial dilution with $R^2 > 0.95$.

### 2.7. Pharmacokinetic (PK) study design

For PK studies, groups of Balb/C mice (n = 3) were injected intraperitoneally with doses of 5 mg/kg or 25 mg/kg of body weight of TPB in 5% dextrose, plasma was collected from the animals at various times post-injection and stored at −80 °C until analysis by LC-MS/MS for TPB concentrations. Plasma drug levels were subjected to non-compartmental analysis (WinNonlin ver. 6.4 Certera Inc., Princeton, N.J.). The predicted steady-state levels > 500 ng/ml were estimated using a twelve h dosing of 25 mg/kg dose of the compound in mice.

### 2.8. Determination of drug concentration in plasma

TPB was dissolved in DMSO at 1 mg/ml. Working standard solutions were then prepared in 50% methanol in water from the stock solution. Standards (an eight-point calibration curve) and quality controls (at three levels) were prepared by spiking the working standard solutions to blank mouse plasma. One hundred µl aliquot of plasma was mixed with 25 µl of internal standard spiking solution (rilpivirine 1000 ng/ml in 50% acetonitrile in water), 1.5 ml ethyl acetate was added and vortexed vigorously for 15 min. The tubes were centrifuged at 1700 × *g* for 5 min and 1.3 ml supernatant was evaporated to dryness under a stream of nitrogen at 40 °C. The dried extract was reconstituted with 0.1 ml of 50% acetonitrile in water and 5 µl was injected into the LC-MS/MS instrument. The dynamic range of the method was 25–4000 ng/ml.

An Agilent 1200 HPLC system (Agilent Technologies, CA, USA) coupled with AB Sciex API 3200 Q Trap with an electrospray ionization source (Applied Biosystems, Foster City, CA, USA) was used. The mass transitions m/z 541.2 → 330.2 and 541.2 → 212.2 for analyte and m/z 367.2 → 195.2 for internal standard were monitored. Chromatographic separation was carried out on Phenomenex Synergi Polar-RP (150 × 2.0 mm, 4µ) column with isocratic mobile phase consisting of 0.1% formic acid in water (A) and 0.1% formic acid in acetonitrile (B) (20:80 v/v) at a flow rate of 0.5 ml/min. The retention times of analyte and internal standard were 2 and 1.2 min respectively.

### 2.9. Viral inhibition test in mice

Balb/C mice were obtained from the Jackson Laboratory (Bar Harbor, ME, USA). After acclimatization for four days, groups of animals (n = 6 per group) were injected intraperitoneally with 25 mg/kg body weight dose of TPB diluted in saline or saline alone (no drug control). Following three injections at 12 h intervals, 500 PFU of PRVABC59 virus diluted in PBS was inoculated into each mouse by the subcutaneous (SC) route. Blood was collected by retro-orbital bleeding under anesthesia at days 2, 3, 4, 5, and 6 post-infection. Viral genome copies in the plasma were determined by RT-qPCR.

### 2.10. Statistical analysis

Data were analyzed using GraphPad Prism software version 6.0. Unpaired two-tailed Student's t-test for pairwise comparison between the groups to determine significant differences in viral loads (RNA levels and infectious titer) was performed. Data were represented as means ( ± SEM).

### 2.11. Ethics statement

All procedures involving animals were conducted in accordance with the guidelines established in the Guide for Care and Use of Laboratory Animals of the National Institutes of Health, USA. The protocol was approved by the Institutional Animal Care and Use Committee at the University of Nebraska-Lincoln. Animals were housed in Life Sciences Annex building at the University. Mice were anesthetized with isoflurane prior to inoculation and all efforts were made to minimize animal suffering.

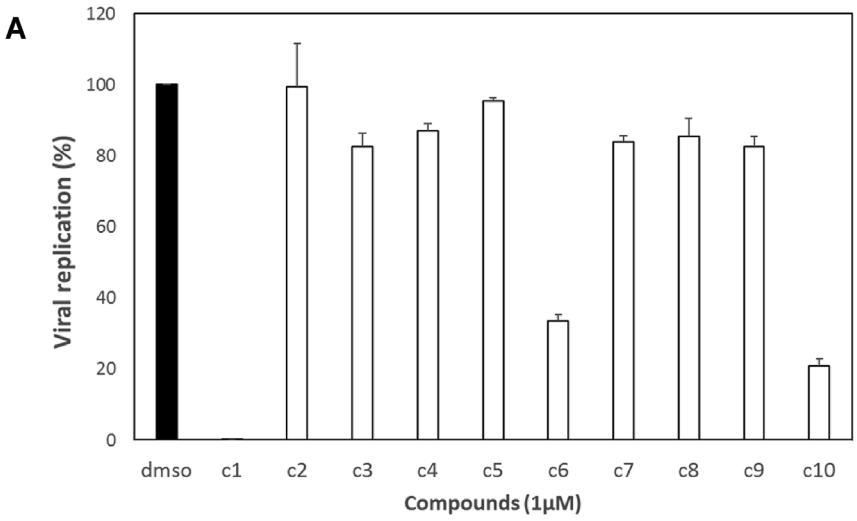


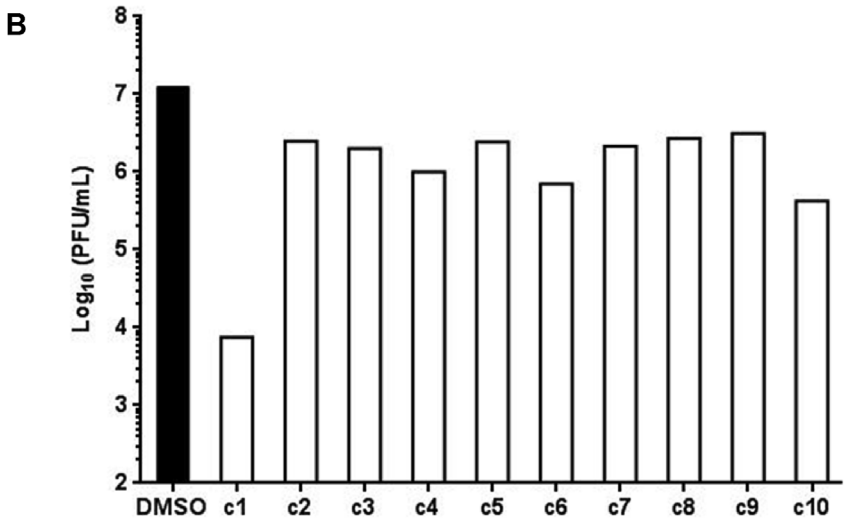


**Fig. 2.** Inhibition of ZIKV replication by the top 10 lead compounds. (A) Viral genome copies in the supernatants of cells infected with PRVABC59 virus in the presence of 1 μM concentration of the ten compounds (c1-c10) or with vehicle (DMSO) alone for 72 h. The data are expressed as % of DMSO-treated control. The experiment was done in triplicate and bars represent ± SEM. (B) Infectious virus titers in the supernatant of cells infected with the virus and incubated with 1 μM concentration of the compounds or with vehicle (DMSO) alone for 96 h.

## 3. Results

### 3.1. In silico screening of a compound library against ZIKV polymerase (RdRp) loops

Since the crystal structure of ZIKV RdRp was not available when this project was initiated, we generated a three-dimensional model of ZIKV RdRp through structural modeling based on the analog of DENV-3 RdRp structure (PDB: 2J7U) (Yap et al., 2007). The choice of the DENV-3 RdRP structure as the template was due to its high level of protein sequence homology (65% identity and 78% similarity) and the high resolution (1.8 Å) of the structure. The predicted ZIKV RdRp structure superimposed closely with the recently solved crystal structure (Duan et al., 2017) of ZIKV RdRp (Fig. S1) with C-alpha atom RMSD of 2.519. The target site appears to fit well and the relative larger RMSD value should be mainly from the flexible loops and the outer layers of the three domains. Like RdRp structures in other flaviviruses, the ZIKV RdRp structure model showed a very similar right-handed architecture with fingers, palm and thumb subdomains (Fig. 1A). Subsequently, we conducted *in silico* screening of a library of 100,000 small molecule compounds against the catalytic active site on the ZIKV RdRp molecule. The active site is in the palm subdomain which is critical for *de novo* RNA synthesis performed by ZIKV RdRp. Based on the *in silico* screening data, the top 10 compounds with highest docking scores are shown in Table 1. The molecular weights of these compounds are also similar (around 500 Da) which are in the appropriate range of druggable compounds.

### 3.2. Cell-based inhibition test of the lead compounds against ZIKV infection

Examination of PRVABC59 ZIKV growth in Vero cells in the presence of 1 μM concentrations of the compounds (c1-c10) showed that c1, 3-chloro-N-[({4-[4-(2-**t**hienylcarbonyl)-1-**p**iperazinyl]phenyl}amino)carbonothioyl]-1-**b**enzothiophene-2-carboxamide (TPB, Fig. 1B), exhibited the highest inhibitory activity among the 10 lead compounds tested. While the ZIKV growth was inhibited (as determined by genome copies in the culture supernatants) by > 99% in cells treated with TPB compared to the vehicle-only treated cells (Fig. 2A), c6 and c10 also inhibited virus growth by nearly 70–80%. Infectious virus yield was inhibited by at least 1000-fold in the presence of 1 μM c1 (Fig. 2B) whereas c6 and c10 inhibited the yield by nearly 10-fold at the same concentrations. Although the majority of the compounds could be readily seen bound to the target site, c1, c6, and c10 appeared to have made additional contacts with the priming loop as well as other regions in the RdRp target site (Fig. S2A and B). From molecular docking analysis, it appears that c1 interacts with residues in the target site of the viral RdRp (Fig. 1C–D). Three hydrogen bonds of TPB are in direct contact with two aspartic acid residues (D535 in motif A and D665 in motif C) in RdRp (Fig. 1C). Since these two aspartic acid residues as well as D665 are highly conserved residues in the target and active site of all RdRps of flaviviruses and play critical roles in coordinating divalent metal ions

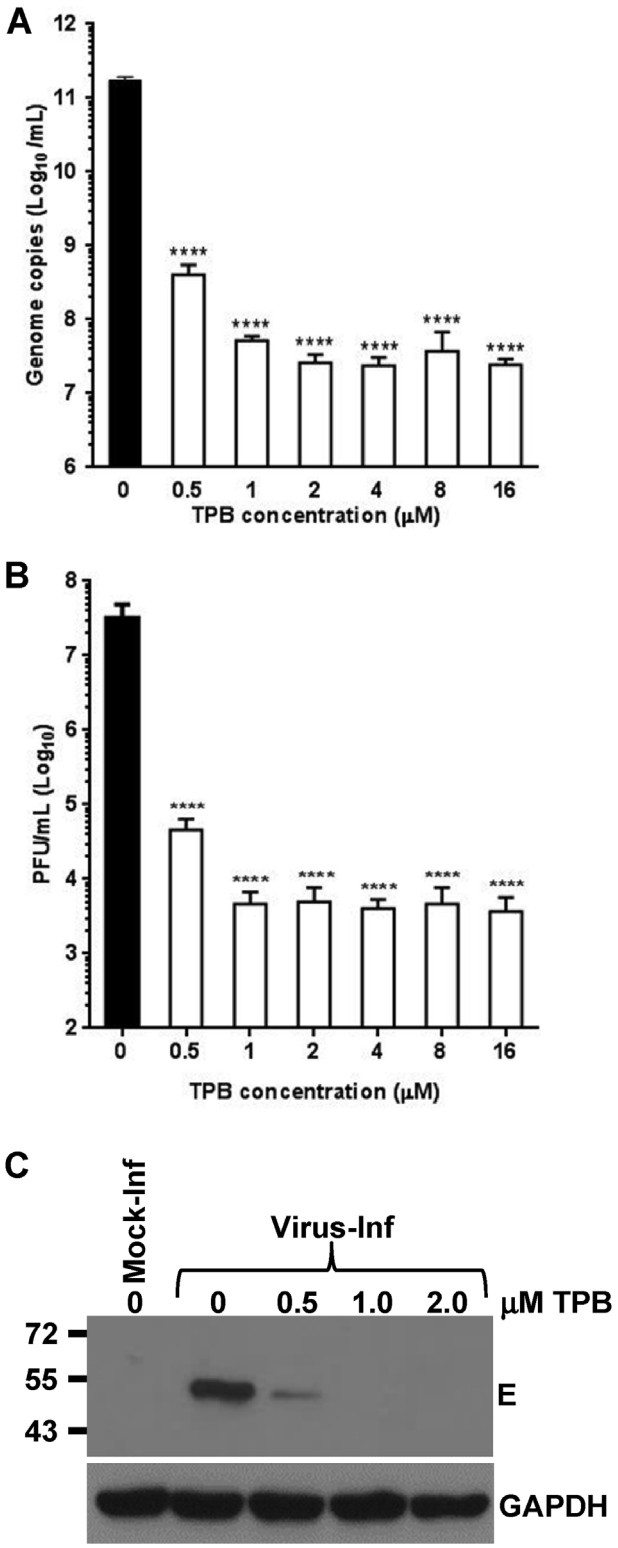


**Fig. 3.** Validation of the antiviral effect of TPB in the μM range. (A) Cells infected with PRVABC59 virus were incubated in the presence of various concentrations of TPB for 96 h. Culture supernatants were titrated for viral genome copies (A) and infectious virus (B). Data are from three independent experiments with error bars showing ± SEM. Statistical analysis was performed using unpaired two-tailed Student's *t*-test to determine significance of difference. ****, $p \leq .001$. (C) Western blot analysis of E protein expression in virus-infected cells in the presence of various concentrations of TPB. Relative mobility of molecular mass markers are shown on the left.

($Mg^{++}$), TPB could potentially be a highly promising anti-ZIKV as well as anti-flavivirus drug candidate. So, from the initial cursory screening studies, TPB was shown to inhibit ZIKV replication significantly.

We then tested the inhibitory activity of TPB in a dose-dependent manner in the μM range. The results show that even at 0.5 μM concentration of TPB, significant inhibitory activity against ZIKV replication was observed. Both genome copy numbers (Fig. 3A) and infectious virus (Fig. 3B) in the supernatants were reduced by over 100-fold at this concentration of TPB. Although TPB at 1 μM reduced virus growth by over 1000-fold, further increase in TPB concentration did not result in further inhibition (Fig. 3A–B). Viral E protein synthesis in infected cells was also significantly inhibited at 0.5 μM TPB and was undetectable at higher concentrations (Fig. 3C). These results suggest that TPB is a potent inhibitor of ZIKV replication.

### 3.3. ZIKV growth inhibition of by TPB

Since we used the contemporary isolate of ZIKV (PRVABC59, isolated from a patient in Puerto Rico in 2015) in our initial studies, we wanted to determine if TBP also has antiviral activity against the historical isolate of the virus. Our results suggest that the MR766 Ugandan isolate was also sensitive to inhibition by TPB at the concentrations tested (Fig. 4A). The extent of MR766 virus growth inhibition appeared to be similar to that of the PRVABC59 virus (Figs. 3 and 4A). Overall, it appears that maximal ZIKV growth inhibition by TPB could be achieved at 1 or 2 μM concentrations and further increase had no significant inhibitory effect, indicating that the TPB inhibitory target is saturable at these concentrations. In addition, not only TPB inhibited ZIKV growth in Vero cells (Fig. 3), but also it inhibited the virus growth in other cells such as human trophoblast cell line HTR-8 (Fig. 4B) as well as the human testicular cell line NTERRA (Fig. 4C) that are known to be the targets of ZIKV infection in humans. Overall, these studies suggest that TBP inhibits both the contemporary and historical isolates of the virus and that the inhibition is not cell-type dependent.

### 3.4. Characterization of TPB antiviral activity in vitro: $IC_{50}$ and $CC_{50}$

#### 3.4.1. Inhibitory concentration 50 ($IC_{50}$) determination

To characterize the anti-ZIKV potency of TPB, we conducted studies to determine the inhibitory concentration 50 ($IC_{50}$). We used serial 2-fold dilutions of TPB and treated the Vero cells infected with PRVABC59. The culture supernatants were assayed for infectious virus by plaque assay and expressed as % virus yield relative to the virus yield without TPB. The data were statistically analyzed and the $IC_{50}$ concentration was determined to be about 94 nM (Fig. 5A). The $IC_{50}$ value of TPB in the 10–100 nM range also suggests that TPB is a strong inhibitor of ZIKV and a potential drug candidate for further development.

#### 3.4.2. Cellular cytotoxicity 50 ($CC_{50}$) determination

Low level of cellular cytotoxicity is an essential criterion for drug development. It also suggests whether the drug's inhibitory effect is independent of cellular cytotoxicity due to the presence of the drug. Therefore, we conducted cell viability assay to determine the cellular cytotoxicity 50 ($CC_{50}$) concentration of TPB. Our results show that $CC_{50}$ of TPB is 19.4 μM (Fig. 5B). The selectivity index 50 ($SI_{50}$, $CC_{50}/IC_{50}$) is calculated to be 206. This high $SI_{50}$ also suggests that TBP is not only a potent inhibitor of ZIKV at sub-micromolar concentrations but is also nontoxic to the cells.

#### 3.4.3. Comparison of TPB inhibition with other known inhibitors of ZIKV

To further compare the potency of TPB relative to other identified ZIKV inhibitors, we examined two inhibitors that have been recently

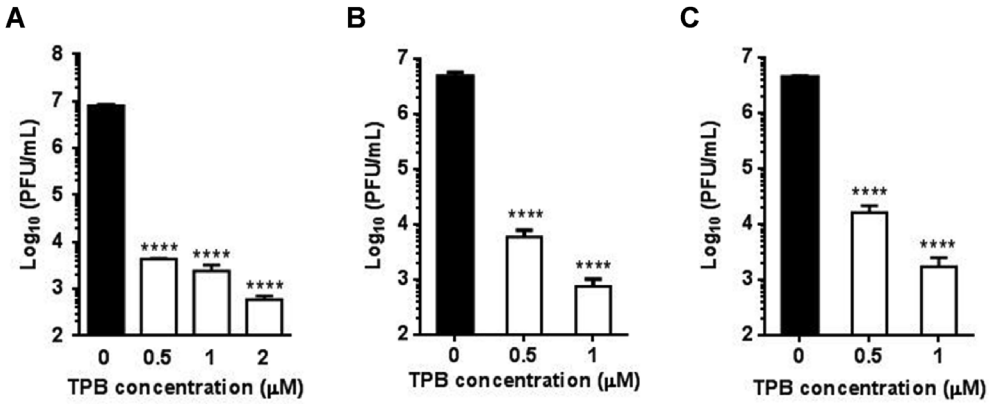


**Fig. 4.** TPB inhibition of ZIKV is strain and cell-type independent. (A) Inhibition of MR766 virus by TPB. The experiments were conducted as in Fig. 3B and data from three independent experiments are presented with error bars representing SEM. PRVABC59 virus growth in HTR-8 (B) and NTERRA (C) cell lines in the presence of TPB. Data from three independent experiments are presented with error bars showing ± SEM. Statistical analysis was performed using unpaired two-tailed Student's t-test to determine significance of difference. ****, $p \leq .001$.

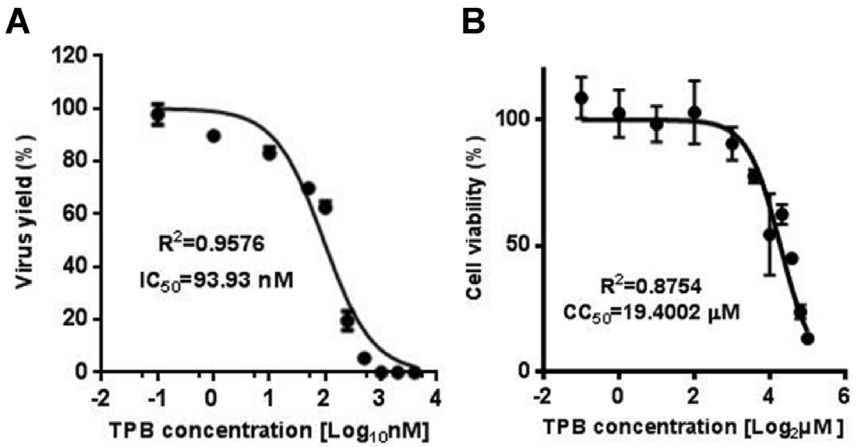


**Fig. 5.** $IC_{50}$ and $CC_{50}$ of TBP. (A) Vero cells in triplicate were infected with PRVABC59 virus and incubated with various concentrations of TPB as shown. Infectious virus titers in the supernatants of the cells at 96 h post-infection were determined by plaque assay and virus yield was expressed as % of TPB-untreated control. Non-linear regression analysis was employed to determine the $IC_{50}$. (B) Vero cells in triplicate were treated with TPB at various concentrations for four days and cell viability was measured based on ATP assay. The luminescence signals were measured at 420 nm using a Microplate Luminometer. Non-linear regression analysis of the data was employed to determine the $CC_{50}$.

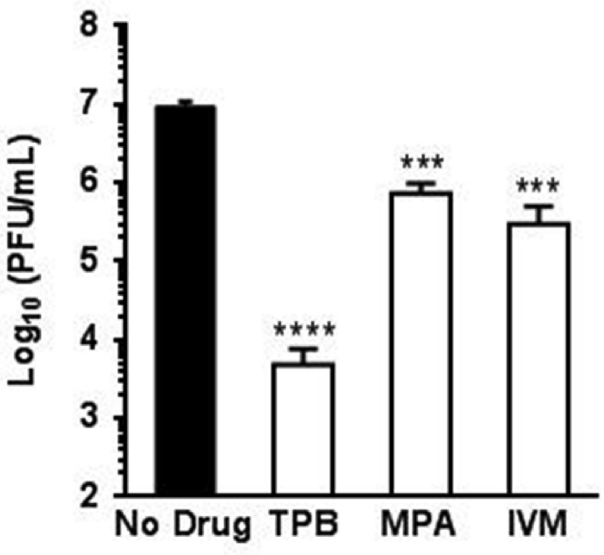


**Fig. 6.** Comparison of TPB inhibitory activity with Mycophenolic acid (MPA) and Ivermectin (IVM). Vero cells were infected with PRVABC59 virus and incubated with TPB (1 μM), MPA (1 μM) and IVM (10 μM). Culture supernatants were collected at 96 h post-infection and assayed for infectious virus. Data presented are from three independent experiments with error bars showing ± SEM. Statistical analysis was performed using unpaired two-tailed Student's t-test to determine significance of difference. ***, $p \leq .01$; ****, $p \leq .001$.

shown to inhibit ZIKV replication. Mycophenolic acid (MPA) is an immunosuppressant drug used to prevent rejection in organ transplantation and was shown to inhibit DENV RNA replication (Diamond et al., 2002). In a screen of FDA-approved drugs for inhibition of ZIKV infection, MPA at 1 μM was found to inhibit infection of cells *in vitro* by ZIKV by over 99% (Barrows et al., 2016). Likewise, Ivermectin (IVM), an anti-parasitic drug (Omura and Crump, 2017), which also inhibits YFV infection (Mastrangelo et al., 2012), was found to inhibit ZIKV infection strongly at 10 μM (Barrows et al., 2016). A side-by-side comparison of the inhibitory potency of TPB with MPA and IVM shows that while TPB inhibited ZIKV yield by over 1000-fold, MPA and IVM inhibited virus yield by approximately 10- to 20-fold (Fig. 6). These results suggest that TPB is more potent in inhibiting ZIKV as compared to MPA or IVM.

### 3.5. Antiviral activity of TPB in vivo

Since TPB was found to be a potent inhibitor of ZIKV replication *in vitro*, we wanted to examine if it also inhibits virus replication and viremia in an immunocompetent mouse model. Although immunodeficient mice models have been developed to study ZIKV pathogenesis and drug development (Julander et al., 2017; Lazear et al., 2016; Rossi et al., 2016; Zmurko et al., 2016), less expensive immunocompetent mice models with limited clinical manifestations have also been used to examine viremia in vaccine studies (Larocca et al., 2016). Therefore, we first conducted a pharmacokinetics (PK) analysis of TPB in immunocompetent Balb/C mice to examine the stability and *in vivo* retention of the drug. The results of PK studies suggest that TPB is retained in the mouse plasma at approximately 100 ng/ml level 10–12 h post-injection at the two doses tested (Fig. 7A). Based on non-compartment analysis of the data, it was estimated that steady-state levels > 500 ng/ml of TPB (~1 μM) could be achieved using a twelve hour dosing at 25 mg/kg dose of the compound in mice. To examine the effect of the drug on ZIKV growth in mice, groups of mice (n = 6) were

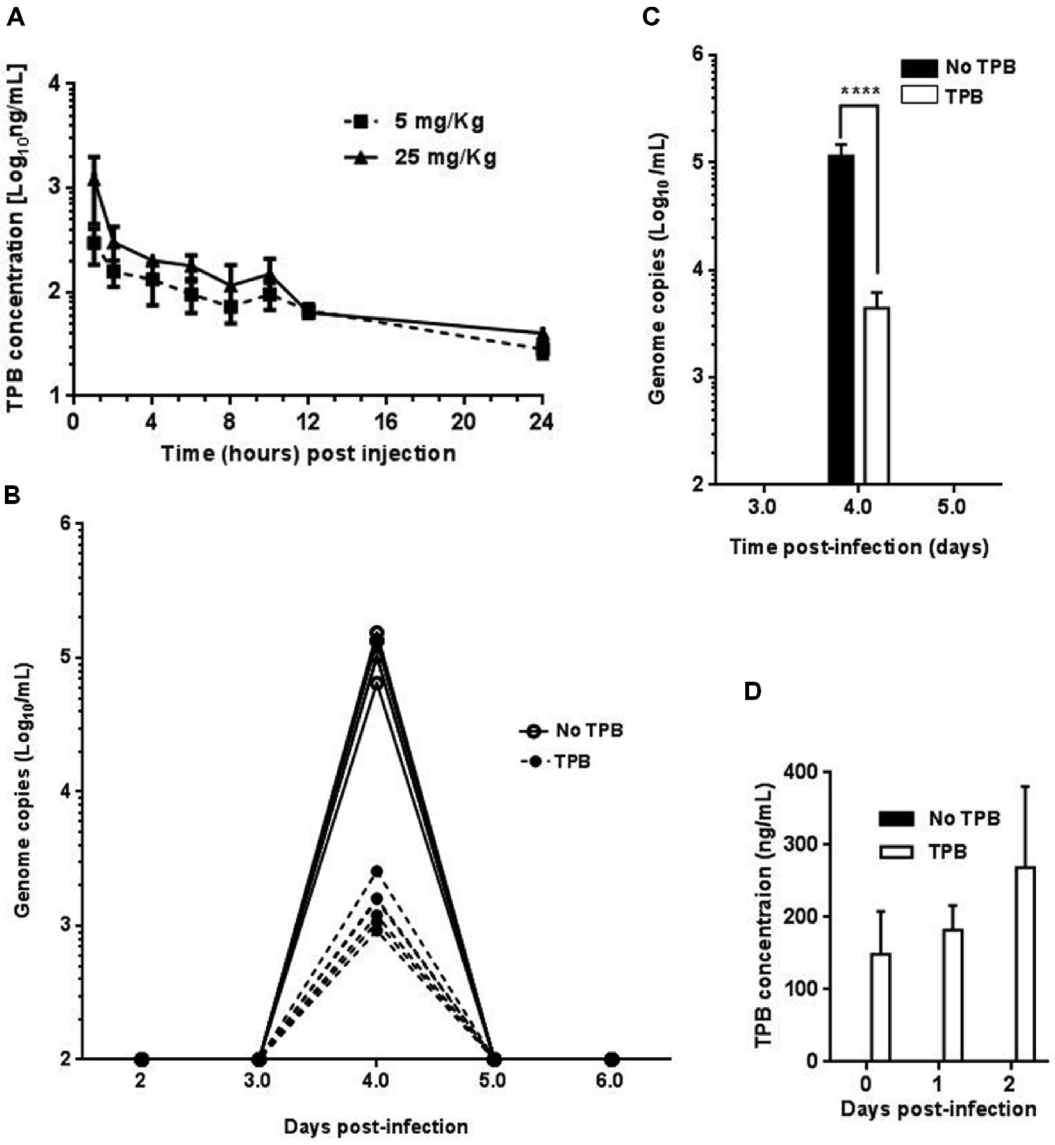


**Fig. 7.** Inhibitory efficacy of TPB in mice. (A) Pharmacokinetics (PK) analysis of TPB in mice using two different doses as shown. (B) Genome copies at various days post-infection in the plasma of individual mice treated without (continuous lines) or with (discontinuous lines) TPB. (C) Data from the mice groups in panel B. Error bars show ± SEM. Statistical analysis was performed using unpaired two-tailed Student's t-test to determine significance of difference. ****, $p \leq .001$. (D) TPB mean concentrations in mice plasma at various days post-infection. Error bars show ± SEM.

injected with the drug at 25 mg/kg dose and subsequently infected with 500 PFU of ZIKV. Virus load in the plasma of the animals at 24 h intervals was determined. Results of virus growth (genome copies) in individual animals (Fig. 7B) show that these immunocompetent mice supported transient ZIKV growth and the level of viral RNA detected on day 4 post-infection was nearly 40-fold lower in mice injected with the drug as compared to the group injected with the vehicle (5% dextrose) alone (Fig. 7C). The transient nature of viremia in these animals has also been noted previously (Larocca et al., 2016; Yu et al., 2017). The level of TPB in the plasma on average reached nearly 270 ng/ml by 2 days post-infection (Fig. 7D). Although this level of TPB was not optimal for maximal virus growth inhibition as observed under *in vitro* conditions, the results suggest that TPB exerts significant growth inhibition of ZIKV *in vivo*.

## 4. Discussion

Through *in silico* screening of a library of 100,000 small molecules, we identified TPB as a potential anti-ZIKV drug candidate. Subsequent *in vitro* and *in vivo* studies demonstrated that TPB exhibits potent inhibitory activity against ZIKV at sub-micromolar concentrations. The inhibitory activity was shown to be against both the African and Asian genotypes representing the historical and contemporary isolates of the virus. In addition, the inhibitory effect of TPB is cell-type independent at least in the cells tested in this study. The $IC_{50}$ and $CC_{50}$ of TPB were determined to be 94 nM and 19.4 μM, respectively, yielding an $SI_{50}$ value of over 200. Such high $SI_{50}$ value suggests that TPB has a strong potential for an effective anti-ZIKV drug with little to no cytotoxicity.

TPB is a non-nucleoside compound which makes it more valuable in the drug development field since non-nucleoside inhibitors (NNI) of viral RdRps are considered to inhibit through allosteric effect by blocking RNA replication/transcription. Thus, they are more selective for viral targets only and with significantly less side-effects (Lim et al., 2015, 2016; Malet et al., 2008). Furthermore, since TPB was docked to the active site of the ZIKZ RdRp forming three hydrogen bonds in direct contact with two aspartic acid residues (D535 in motif A and D665 in motif C) in RdRp (Fig. 1C), it makes this compound a promising anti-ZIKV drug candidate. The aspartic acid residues (D535/D665 or D535/D665/D666) are highly conserved in the active sites of all RdRps of flaviviruses and play essential roles in coordinating with two divalent

metal ions ($Mg^{++}$) for initiation of ribonucleotide polymerization (Butcher et al., 2001; Choi and Rossmann, 2009; Duan et al., 2017; Godoy et al., 2017; Ng et al., 2008; Yap et al., 2007; Zhao et al., 2017). The binding of TPB to these active site residues and possibly blocking of this active site must be very efficient, which may likely explain the potent inhibitory activity of TPB at sub-micromolar concentrations. However, further work on *in vitro* binding of the polymerase with TPB leading to inhibition of RdRp activity needs to be validated experimentally. Additionally, the binding of TPB to NS5 may alter its interaction with other NS proteins involved in virus genome replication, leading to inhibition. Future studies will reveal the mechanism of inhibition of NS5 function by TPB.

We have evaluated TPB toxicity using ATP-based as well as MTT-based (data not shown) assays. Results from both methods were similar and suggested that there were no observed cellular toxicity *in vitro*. When TPB was administered at 25 mg/kg dose, all mice appeared normal over a six-day period. However, if TPB is to be tested for its potential use as a drug candidate, detailed investigation needs to be conducted to assess its toxicity *in vivo*.

Since the ZIKV RdRp model used in this research was generated from homology modeling using the DENV-3 RdRp structure, it is presumed that TPB and other lead compounds could be tested for anti-DENV activity. Additionally, for other flaviviruses such as Japanese Encephalitis Virus (JEV) for which the RdRp has the highest homology level in protein sequence to that of ZIKV RdRp (Lu and Gong, 2013; Upadhyay et al., 2017), it is possible that TPB could also be effective against JEV. Although there are some observed structural differences such as in the Ring motif F, the active site is highly conserved in the flavivirus RdRps. Of special note here are the two aspartic acid residues (D535/D665) that are present in the catalytic pocket of RdRp that provide a foundation for TPB binding.

In conclusion, through the *in silico* screening approach, we have identified a non-nucleotide compound, TPB, which shows a potent inhibitory activity against ZIKV infection *in vitro* as well as *in vivo*. TPB is a novel non-nucleoside inhibitor targeting the active site of ZIKV RdRp. This compound also opens the perspectives for anti-flavivirus drug design.

## Acknowledgments

This work was supported by funds provided to A.K.P. from the University of Nebraska-Lincoln. The virtual screens of the compound library were completed utilizing the Holland Computing Center of the University of Nebraska, which receives support from the Nebraska Research Initiative.

## Appendix A. Supplementary data

Supplementary data related to this article can be found at http://dx.doi.org/10.1016/j.antiviral.2017.12.016.

## References

Aliota, M.T., Bassit, L., Bradrick, S.S., Cox, B., Garcia-Blanco, M.A., Gavegnano, C., Friedrich, T.C., Golos, T.G., Griffin, D.E., Haddow, A.D., Kallas, E.G., Kitron, U., Lecuit, M., Magnani, D.M., Marrs, C., Mercer, N., McSweegan, E., Ng, L.F.P., O'Connor, D.H., Osorio, J.E., Ribeiro, G.S., Ricciardi, M., Rossi, S.L., Saade, G., Schinazi, R.F., Schott-Lerner, G.O., Shan, C., Shi, P.Y., Watkins, D.I., Vasilakis, N., Weaver, S.C., 2017. Zika in the Americas, year 2: what have we learned? what gaps remain? a report from the global virus network. Antivir. Res. 144, 223–246.

Annamalai, A.S., Pattnaik, A., Sahoo, B.R., Muthukrishnan, E., Natarajan, S.K., Steffen, D., Vu, H.L.X., Delhon, G., Osorio, F.A., Petro, T.M., Xiang, S.H., Pattnaik, A.K., 2017. Zika virus encoding non-glycosylated envelope protein is attenuated and defective in neuroinvasion. J. Virol. 91 e01348–17.

Avelino-Silva, V.I., Martin, J.N., 2016. Association between Guillain-Barre syndrome and zika virus infection. Lancet 387, 2599.

Baronti, C., Piorkowski, G., Charrel, R.N., Boubis, L., Leparc-Goffart, I., de Lamballerie, X., 2014. Complete coding sequence of zika virus from a French Polynesia outbreak in 2013. Genome Announc. 2.

Barrows, N.J., Campos, R.K., Powell, S.T., Prasanth, K.R., Schott-Lerner, G., Soto-Acosta, R., Galarza-Munoz, G., McGrath, E.L., Urrabaz-Garza, R., Gao, J., Wu, P., Menon, R., Saade, G., Fernandez-Salas, I., Rossi, S.L., Vasilakis, N., Routh, A., Bradrick, S.S., Garcia-Blanco, M.A., 2016. A screen of FDA-approved drugs for inhibitors of zika virus infection. Cell Host Microbe 20, 259–270.

Butcher, S.J., Grimes, J.M., Makeyev, E.V., Bamford, D.H., Stuart, D.I., 2001. A mechanism for initiating RNA-dependent RNA polymerization. Nature 410, 235–240.

Carteaux, G., Maquart, M., Bedet, A., Contou, D., Brugieres, P., Fourati, S., Cleret de Langavant, L., de Broucker, T., Brun-Buisson, C., Leparc-Goffart, I., Mekontso Dessap, A., 2016. Zika virus associated with meningoencephalitis. N. Engl. J. Med. 374, 1595–1596.

Cauchemez, S., Besnard, M., Bompard, P., Dub, T., Guillemette-Artur, P., Eyrolle-Guignot, D., Salje, H., Van Kerkhove, M.D., Abadie, V., Garel, C., Fontanet, A., Mallet, H.P., 2016. Association between Zika virus and microcephaly in French Polynesia, 2013-15: a retrospective study. Lancet 387, 2125–2132.

Chan, J.F., Choi, G.K., Yip, C.C., Cheng, V.C., Yuen, K.Y., 2016. Zika fever and congenital Zika syndrome: an unexpected emerging arboviral disease. J. Infect. 72, 507–524.

Che, P., Wang, L., Li, Q., 2009. The development, optimization and validation of an assay for high throughput antiviral drug screening against dengue virus. Int. J. Clin. Exp. Med. 2, 363–373.

Choi, K.H., Rossmann, M.G., 2009. RNA-dependent RNA polymerases from flaviviridae. Curr. Opin. Struct. Biol. 19, 746–751.

Coutard, B., Barral, K., Lichiere, J., Selisko, B., Martin, B., Aouadi, W., Lombardia, M.O., Debart, F., Vasseur, J.J., Guillemot, J.C., Canard, B., Decroly, E., 2017. Zika virus methyltransferase: structure and functions for drug design perspectives. J. Virol. 91, e02202–e02216.

Coyne, C.B., Lazear, H.M., 2016. Zika virus - reigniting the TORCH. Nat. Rev. Microbiol. 14, 707–715.

Cugola, F.R., Fernandes, I.R., Russo, F.B., Freitas, B.C., Dias, J.L., Guimaraes, K.P., Benazzato, C., Almeida, N., Pignatari, G.C., Romero, S., Polonio, C.M., Cunha, I., Freitas, C.L., Brandao, W.N., Rossato, C., Andrade, D.G., Faria Dde, P., Garcez, A.T., Buchpigel, C.A., Braconi, C.T., Mendes, E., Sall, A.A., Zanotto, P.M., Peron, J.P., Muotri, A.R., Beltrao-Braga, P.C., 2016. The Brazilian Zika virus strain causes birth defects in experimental models. Nature 534, 267–271.

Deseda, C.C., 2017. Epidemiology of zika. Curr. Opin. Pediatr. 29, 97–101.

Diamond, M.S., Zachariah, M., Harris, E., 2002. Mycophenolic acid inhibits dengue virus infection by preventing replication of viral RNA. Virology 304, 211–221.

Dick, G.W., Kitchen, S.F., Haddow, A.J., 1952. Zika virus. I. Isolations and serological specificity. Trans. Roy. Soc. Trop. Med. Hyg. 46, 509–520.

Duan, W., Song, H., Wang, H., Chai, Y., Su, C., Qi, J., Shi, Y., Gao, G.F., 2017. The crystal structure of Zika virus NS5 reveals conserved drug targets. EMBO J. 36, 919–933.

Fauci, A.S., Morens, D.M., 2016. Zika virus in the americas–yet another arbovirus threat. N. Engl. J. Med. 374, 601–604.

Godoy, A.S., Lima, G.M., Oliveira, K.I., Torres, N.U., Maluf, F.V., Guido, R.V., Oliva, G., 2017. Crystal structure of Zika virus NS5 RNA-dependent RNA polymerase. Nat. Commun. 8, 14764.

Gulland, A., 2016. Zika virus is a global public health emergency, declares WHO. BMJ 352, i657.

Julander, J.G., Siddharthan, V., Evans, J., Taylor, R., Tolbert, K., Apuli, C., Stewart, J., Collins, P., Gebre, M., Neilson, S., Van Wettere, A., Lee, Y.M., Sheridan, W.P., Morrey, J.D., Babu, Y.S., 2017. Efficacy of the broad-spectrum antiviral compound BCX4430 against Zika virus in cell culture and in a mouse model. Antivir. Res. 137, 14–22.

Larocca, R.A., Abbink, P., Peron, J.P., Zanotto, P.M., Iampietro, M.J., Badamchi-Zadeh, A., Boyd, M., Ng'ang'a, D., Kirilova, M., Nityanandam, R., Mercado, N.B., Li, Z., Moseley, E.T., Bricault, C.A., Borducchi, E.N., Giglio, P.B., Jetton, D., Neubauer, G., Nkolola, J.P., Maxfield, L.F., De La Barrera, R.A., Jarman, R.G., Eckels, K.H., Michael, N.L., Thomas, S.J., Barouch, D.H., 2016. Vaccine protection against Zika virus from Brazil. Nature 536, 474–478.

Lazear, H.M., Diamond, M.S., 2016. Zika virus: new clinical syndromes and its emergence in the Western hemisphere. J. Virol. 90, 4864–4875.

Lazear, H.M., Govero, J., Smith, A.M., Platt, D.J., Fernandez, E., Miner, J.J., Diamond, M.S., 2016. A mouse model of zika virus pathogenesis. Cell Host Microbe 19, 720–730.

Lim, S.P., Noble, C.G., Seh, C.C., Soh, T.S., El Sahili, A., Chan, G.K., Lescar, J., Arora, R., Benson, T., Nilar, S., Manjunatha, U., Wan, K.F., Dong, H., Xie, X., Shi, P.Y., Yokokawa, F., 2016. Potent allosteric dengue virus NS5 polymerase inhibitors: mechanism of action and resistance profiling. PLoS Pathog. 12, e1005737.

Lim, S.P., Noble, C.G., Shi, P.Y., 2015. The dengue virus NS5 protein as a target for drug discovery. Antivir. Res. 119, 57–67.

Lu, G., Gong, P., 2013. Crystal Structure of the full-length Japanese encephalitis virus NS5 reveals a conserved methyltransferase-polymerase interface. PLoS Pathog. 9, e1003549.

Malet, H., Masse, N., Selisko, B., Romette, J.L., Alvarez, K., Guillemot, J.C., Tolou, H., Yap, T.L., Vasudevan, S., Lescar, J., Canard, B., 2008. The flavivirus polymerase as a target for drug discovery. Antivir. Res. 80, 23–35.

Mastrangelo, E., Pezzullo, M., De Burghgraeve, T., Kaptein, S., Pastorino, B., Dallmeier, K., de Lamballerie, X., Neyts, J., Hanson, A.M., Frick, D.N., Bolognesi, M., Milani, M., 2012. Ivermectin is a potent inhibitor of flavivirus replication specifically targeting NS3 helicase activity: new prospects for an old drug. J. Antimicrob. Chemother. 67, 1884–1894.

Mecharles, S., Herrmann, C., Poullain, P., Tran, T.H., Deschamps, N., Mathon, G., Landais, A., Breurec, S., Lannuzel, A., 2016. Acute myelitis due to Zika virus infection. Lancet 387, 1481.

Miner, J.J., Diamond, M.S., 2017. Zika virus pathogenesis and tissue tropism. Cell Host Microbe 21, 134–142.

Mlakar, J., Korva, M., Tul, N., Popovic, M., Poljsak-Prijatelj, M., Mraz, J., Kolenc, M.,

Resman Rus, K., Vesnaver Vipotnik, T., Fabjan Vodusek, V., Vizjak, A., Pizem, J., Petrovec, M., Avsic Zupanc, T., 2016. Zika virus associated with microcephaly. N. Engl. J. Med. 374, 951–958.
Munoz, L.S., Barreras, P., Pardo, C.A., 2016. Zika virus-associated neurological disease in the adult: Guillain-Barre syndrome, encephalitis, and myelitis. Semin. Reprod. Med. 34, 273–279.
Nascimento, O.J.M., Frontera, J.A., Amitrano, D.A., Bispo de Filippis, A.M., Da Silva, I.R.F., Group, R.-G.-Z.R., 2017. Zika virus infection-associated acute transient polyneuritis. Neurology 88, 2330–2332.
Ng, K.K., Arnold, J.J., Cameron, C.E., 2008. Structure-function relationships among RNA-dependent RNA polymerases. Curr. Top. Microbiol. Immunol. 320, 137–156.
Omura, S., Crump, A., 2017. Ivermectin and malaria control. Malar. J. 16, 172.
Parra, B., Lizarazo, J., Jimenez-Arango, J.A., Zea-Vera, A.F., Gonzalez-Manrique, G., Vargas, J., Angarita, J.A., Zuniga, G., Lopez-Gonzalez, R., Beltran, C.L., Rizcala, K.H., Morales, M.T., Pacheco, O., Ospina, M.L., Kumar, A., Cornblath, D.R., Munoz, L.S., Osorio, L., Barreras, P., Pardo, C.A., 2016. Guillain-barre syndrome associated with zika virus infection in Colombia. N. Engl. J. Med. 375, 1513–1523.
Perera, R., Kuhn, R.J., 2008. Structural proteomics of dengue virus. Curr. Opin. Microbiol. 11, 369–377.
Ramharack, P., Soliman, M.E.S., 2017. Zika virus NS5 protein potential inhibitors: an enhanced in silico approach in drug discovery. J. Biomol. Struct. Dynam. 1–16.
Rather, I.A., Kumar, S., Bajpai, V.K., Lim, J., Park, Y.H., 2017. Prevention and control strategies to counter ZIKA epidemic. Front. Microbiol. 8, 305.
Roos, R.P., 2016. Zika virus-a public health emergency of international concern. J. Neurol. 73, 1395–1396.
Rossi, S.L., Tesh, R.B., Azar, S.R., Muruato, A.E., Hanley, K.A., Auguste, A.J., Langsjoen, R.M., Paessler, S., Vasilakis, N., Weaver, S.C., 2016. Characterization of a novel murine model to study zika virus. Am. J. Trop. Med. Hyg. 94, 1362–1369.
Salam, A.P., Rojek, A., Dunning, J., Horby, P.W., 2017. Clinical trials of therapeutics for the prevention of congenital zika virus disease: challenges and potential solutions. Ann. Intern. Med. 166, 725–732.
Shan, C., Xie, X., Barrett, A.D., Garcia-Blanco, M.A., Tesh, R.B., Vasconcelos, P.F., Vasilakis, N., Weaver, S.C., Shi, P.Y., 2016. Zika virus: diagnosis, therapeutics, and vaccine. Adv. Infect. Dis. 2, 170–172.
Shi, Y., Gao, G.F., 2017. Structural biology of the zika virus. Trends Biochem. Sci. 42, 443–456.
Upadhyay, A.K., Cyr, M., Longenecker, K., Tripathi, R., Sun, C., Kempf, D.J., 2017. Crystal structure of full-length Zika virus NS5 protein reveals a conformation similar to Japanese encephalitis virus NS5. Acta Crystallogr. F Struct. Biol. Commun. 73, 116–122.
Wang, B., Tan, X.F., Thurmond, S., Zhang, Z.M., Lin, A., Hai, R., Song, J., 2017. The structure of Zika virus NS5 reveals a conserved domain conformation. Nat. Commun. 8, 14763.
Weaver, S.C., Costa, F., Garcia-Blanco, M.A., Ko, A.I., Ribeiro, G.S., Saade, G., Shi, P.Y., Vasilakis, N., 2016. Zika virus: history, emergence, biology, and prospects for control. Antivir. Res. 130, 69–80.
Webb, B., Sali, A., 2014. Protein structure modeling with MODELLER. Meth. Mol. Biol. 1137, 1–15.
Yap, T.L., Xu, T., Chen, Y.L., Malet, H., Egloff, M.P., Canard, B., Vasudevan, S.G., Lescar, J., 2007. Crystal structure of the dengue virus RNA-dependent RNA polymerase catalytic domain at 1.85-angstrom resolution. J. Virol. 81, 4753–4765.
Yu, J., Liu, X., Ke, C., Wu, Q., Lu, W., Qin, Z., He, X., Liu, Y., Deng, J., Xu, S., Li, Y., Zhu, L., Wan, C., Zhang, Q., Xiao, W., Xie, Q., Zhang, B., Zhao, W., 2017. Effective suckling C57BL/6, Kunming, and BALB/c mouse models with remarkable neurological manifestation for zika virus infection. Viruses 9, e165.
Yuan, Z., Kang, G., Ma, F., Lu, W., Fan, W., Fennessey, C.M., Keele, B.F., Li, Q., 2016. Recapitulating cross-species transmission of simian immunodeficiency virus SIVcpz to humans by using humanized BLT mice. J. Virol. 90, 7728–7739.
Zhao, B., Yi, G., Du, F., Chuang, Y.C., Vaughan, R.C., Sankaran, B., Kao, C.C., Li, P., 2017. Structure and function of the Zika virus full-length NS5 protein. Nat. Commun. 8, 14762.
Zmurko, J., Marques, R.E., Schols, D., Verbeken, E., Kaptein, S.J., Neyts, J., 2016. The viral polymerase inhibitor 7-deaza-2'-C-methyladenosine is a potent inhibitor of in vitro zika virus replication and delays disease progression in a robust mouse infection model. PLoS Neglected Trop. Dis. 10, e0004695.